Hindawi

Research Article

Preparation of Tetra Pak-Based Hydrochars for Cleaning Water Polluted by Heavy Metal Ions: Physicochemical Properties and Removal Mechanism

Evelyn Mirelle Valdés-Rodríguez,[1] **Leonardo Frias-Gasparri,**[2]
Didilia Ileana Mendoza-Castillo ⓘ **,**[1,3] **Verónica Janeth Landin-Sandoval,**[2]
and Adrián Bonilla-Petriciolet ⓘ [1]

[1]*Instituto Tecnológico de Aguascalientes, Aguascalientes 20256, Mexico*
[2]*Universidad Tecnológica Metropolitana de Aguascalientes, Aguascalientes 20126, Mexico*
[3]*CONACYT, Ciudad de México 03940, Mexico*

Correspondence should be addressed to Didilia Ileana Mendoza-Castillo; dimendozaca@conacyt.mx

This paper addresses the analysis of hydrothermal carbonization of Tetra Pak residues using diluted sulfuric acid to obtain hydrochars for cleaning water polluted by heavy metal ions. The hydrochar samples were prepared under different carbonization conditions, and a detailed study of their composition, textural parameters, and surface functionalities was performed. It was found that the hydrothermal carbonization and dwell time of the Tetra Pak wastes significantly affected the composition of the hydrochars. These hydrochar samples contained oxygenated functional groups and aluminum-silicon moieties that were responsible for the Pb^{2+}, Zn^{2+}, and Hg^{2+} adsorption. The removal of these heavy metal ions using Tetra Pak hydrochars was an endothermic and multi-ionic process. Hydrothermal carbonization is a promising approach to improve Tetra Pak waste management, generating materials with interesting properties for addressing the problem of wastewater and industrial effluent depollution.

1. Introduction

Integral waste management in urban and rural sectors is fundamental to meet the goals of sustainable development of society. Various strategies have been implemented to valorize solid residues and obtain value-added products [1, 2]. This approach allows the minimization of waste generation and its corresponding environmental impact and the reduction of its management costs according to the circular economy perspective. To date, novel materials for addressing depollution problems (e.g., water and air cleaning) have been synthesized from different wastes and residues [3, 4].

In particular, the Tetra Pak wastes are generated worldwide because of the extensive application of this packaging container in the food industry. They can be classified as composites containing aluminum, paperboard, and polyethylene [5, 6]. Consequently, their recycling and reuse present different challenges, where the separation of the main Tetra Pak components is difficult and relatively costly [7]. The recycling of residual Tetra Pak containers has mainly focused on cellulose recovery [8–11]. The extraction of cellulose fibers from Tetra Pak waste can be performed via sulfuric acid treatment, where the properties of the final product can be tailored for specific applications [12]. This recycled cellulose can be utilized to prepare different products [9, 11, 12].

Other viable options, both financially and industrially, for the valorization and exploitation of Tetra Pak packing components have been addressed in recent studies [6, 13]. These include the preparation of recycled polymers [14],

flame-retardant copolymers [6], catalytic production of bio-oil [7], and synthesis of adsorbents for water cleaning [5, 15]. For example, the application of different solvents allows the separation of the main components of Tetra Pak waste via delamination [16]. Wang et al. [7] studied the production of bio-oil and other subproducts, including a solid phase that was not physiochemically characterized, via the catalytic hydrothermal liquefaction of Tetra Pak residues.

Pyrolysis and hydrothermal carbonization are thermochemical conversion routes for valorizing Tetra Pak residues [5, 15, 17, 18]. They can be utilized to prepare porous materials for different applications, including water depollution. However, the contributions in this direction are limited. For the case of pyrolysis, Ding et al. [15] analyzed the arsenic removal using a Tetra Pak-based char. The packing container wastes were pretreated with acid and pyrolyzed at 600°C. This adsorbent removed 24–33 mg/g of arsenic from polluted aqueous solutions. Another study showed that the pyrolysis of Tetra Pak residues allows the preparation of new materials for the mercury adsorption [5]. These adsorbents exhibited high adsorption properties to remove this toxic metal ion at 30–40°C and pH 1.5–4. Recently, Zmijková et al. [18] reported the Tetra Pak pyrolysis at 400–700°C to obtain char samples, which were not evaluated for the water depollution. Herein, it is convenient to point out that the main disadvantage of pyrolysis as a valorization route is associated with the high temperatures (>600°C) required to obtain these adsorbents causing the corresponding increase in the energy consumption and production cost. On the other hand, the hydrothermal carbonization of Tetra Pak containers has been addressed in a few studies [13, 17, 18]. Lokahita et al. [13] analyzed the hydrothermal carbonization of Tetra Pak at 200–240°C for 60 min. The hydrochars obtained under different conditions were partially characterized, but their application in water treatment was not assessed. Hydrothermal carbonization of Tetra Pak residues at 160–240°C for 40–120 min was also studied by Muñoz-Batista et al. [17] to prepare hydrochars. Some properties of these materials were compared with those of Tetra Pak chars obtained via pyrolysis at 400–600°C. However, these authors did not report the adsorption properties of hydrochars and chars for the removal of water pollutants.

This literature overview clearly shows that the Tetra Pak adsorbents obtained from pyrolysis have been introduced to remove a few toxic pollutants (i.e., arsenic and mercury) [5, 15], while the adsorption and surface properties of Tetra Pak-based hydrochars have not been reported to remove contaminants commonly found in wastewater. This is despite the fact that the hydrothermal carbonization can operate under milder conditions, favoring the energy consumption during waste conversion. This highlights the necessity of studying the main physicochemical characteristics and removal performance of these hydrochars with the aim of establishing their potential to depollute wastewater and industrial effluents.

This study analyzed the hydrothermal carbonization to valorize Tetra Pak residues and obtain new adsorbents for cleaning water polluted by toxic heavy metals. Tetra Pak-based hydrochars were prepared using diluted H_2SO_4 at different carbonization temperatures and dwell times, and their adsorption properties were assessed for the depollution of aqueous solutions containing zinc (Zn^{2+}), lead (Pb^{2+}), and mercury (Hg^{2+}) ions. Surface properties of these adsorbents were determined using X-ray diffraction, FTIR, SEM/EDX, and N_2 physisorption. The adsorption equilibrium for these heavy metals was studied using the best hydrochars, and a multisite adsorption model was employed to describe and interpret their adsorption mechanisms. The results reported in this paper will contribute to the development of alternatives for the valorization and recycling of residual Tetra Pak containers.

2. Preparation of Tetra Pak-Based Hydrochars, Their Characterization, and Adsorption Properties

2.1. Conditions of Hydrothermal Carbonization of Tetra Pak Residues and Their Characterization. Residual Tetra Pak containers were collected from local markets, washed, dried, and cut to obtain particles with ∼0.67 mm size. An experimental design was utilized to prepare hydrochars under different hydrothermal carbonization conditions for the thermochemical conversion of Tetra Pak wastes and to identify the samples with the best adsorption properties for cleaning water polluted by heavy metal ions. Table 1 shows the 3-level factorial experimental design where the hydrothermal carbonization temperature (180–230°C) and dwell time (6–18 h) were manipulated to analyze their effect on hydrochar adsorption properties. Nine samples were prepared from this experimental design and assessed for Pb^{2+}, Hg^{2+}, and Zn^{2+} removal from aqueous solutions. A stainless-steel reactor (100 mL capacity) was employed for the hydrothermal carbonization of Tetra Pak residues with 0.1 M H_2SO_4 as the reaction medium. The reactor load used in the hydrothermal carbonization was 1 g of Tetra Pak per 3 mL of the acidic solution. The solid product yield was determined for all tested hydrothermal carbonization conditions. The washing (with deionized water) and drying of all hydrochar samples were performed, and their final particle sizes were ∼0.21 mm.

The heavy metal removal properties of hydrochar samples were assessed with batch adsorbers. These studies were carried out with 1 L of aqueous solution (with initial metal concentrations of 1–3 mmol/L) per 2 g of hydrochar sample. The operating conditions for Pb^{2+} and Zn^{2+} adsorption were 30°C and pH 5, respectively, while Hg^{2+} removal was analyzed at pH 4 and 30°C. Preliminary studies indicated that these operating conditions favored the removal of these heavy metal ions thus reducing the adsorption competition caused by H^+ at low pH. Also, these pH values avoided the microprecipitation of tested pollutants; see Figure S1 of Supporting Information. Deionized water and reactive-grade nitrate and chloride salts of Pb^{2+}, Zn^{2+}, and Hg^{2+} were utilized to prepare aqueous solutions for the adsorption experiments. Atomic absorption spectroscopy was used to quantify Zn^{2+}, Hg^{2+}, and Pb^{2+} concentrations in all the solutions. The

TABLE 1: Hydrothermal carbonization conditions used to obtain Tetra Pak-based hydrochars.

Hydrochar sample	Hydrothermal carbonization	
	Temperature (°C)	Dwell time (h)
TP1	180	6
TP2	180	12
TP3	180	18
TP4	200	6
TP5	200	12
TP6	200	18
TP7	230	6
TP8	230	12
TP9	230	18

adsorption capacities were calculated using the material balance of the batch adsorber (see Figure 1). The results and statistical analysis of the experimental design (Table 1) were applied to select the best hydrochar to remove tested contaminants. The adsorption isotherms for Pb^{2+}, Zn^{2+}, and Hg^{2+} were measured employing the hydrochar samples with the highest adsorption properties. These equilibrium studies were conducted at 30 and 40°C under the same operating parameters as those used in the assessment of the experimental design.

The adsorption properties of hydrochars were associated with their main surface properties. The functional groups and crystalline structures of these adsorbents were analyzed via FTIR spectroscopy and X-ray diffraction. FTIR analysis allowed the identification of the main organic surface functionalities of hydrochars, while X-ray diffraction permitted the identification of aluminum moieties and other crystalline compounds on their surfaces. These characterization techniques were also useful for studying the surface chemistry transitions of samples obtained under different hydrothermal carbonization conditions. Elemental analysis was performed using SEM/EDX, and textural parameters of the hydrochars were analyzed via nitrogen physisorption. The pH values at the point of zero charge and the concentrations of the acidic sites were also determined. Figure 2 provides an overview of the equipment and conditions of these analyses.

2.2. Adsorption Isotherms of Pb^{2+}, Hg^{2+}, and Zn^{2+} for the Best Tetra Pak-Based Hydrochars. The equilibrium and thermodynamics of Zn^{2+}, Hg^{2+}, and Pb^{2+} adsorption on the best hydrochars were studied. The experimental adsorption isotherms were quantified at 30 and 40°C, pH 5 (Pb^{2+} and Zn^{2+}) and pH 4 (Hg^{2+}). A hydrochar dosage of 2 g/L and continuous stirring (120 rpm) for 24 h were utilized to reach the adsorption equilibrium in these experiments. The saturation of hydrochar samples was obtained with initial heavy metal concentrations range of 0.05–11 mmol/L. All the adsorption studies were carried out by triplicate, and the average values (with an error ≤5%) are reported in this study. Adsorption enthalpy changes (ΔH, kJ/mol) were calculated using the experimental adsorption isotherms following the procedure described in [5].

2.3. Adsorption Mechanism of Heavy Metals on Tetra Pak-Based Hydrochars. The mechanism of Pb^{2+}, Hg^{2+}, and Zn^{2+} adsorption on Tetra Pak-based hydrochars was analyzed using two adsorption models via a nonlinear regression using the Solver add-in of Microsoft Excel®. The surface chemistry characterization results indicated that the hydrochar samples had different compositions depending on the conditions applied for the hydrothermal carbonization of the Tetra Pak residues; therefore, it was assumed that the removal mechanism of these metallic species occurred via one or two adsorption sites, depending on the adsorbent sample. These adsorption models also hypothesized that these heavy metal ions formed a monolayer on the adsorbent surface [19]. Based on these facts, equation (1) describes a monolayer heavy metal adsorption involving one type of functional group (i.e., one heavy metal-hydrochar interaction energy):

$$q_e = \frac{Ion_{S1} D_{S1}}{1 + \left([Ion]_{hS1} / [Ion]_e \right)^{Ion_{S1}}}, \tag{1}$$

where Ion_{S1} is the number of Pb^{2+}, Hg^{2+}, and Zn^{2+} that can interact with adsorption site 1 from the hydrochar surface, D_{S1} is the density (mmol/g) of adsorption site 1 participating in the heavy metal removal, q_e is the adsorption capacity at equilibrium (mmol/g), $[Ion]_{hS1}$ is the heavy metal ion concentration (mmol/L) at the half saturation condition for adsorption site 1, and $[Ion]_e$ is the equilibrium concentration (mmol/L) of the heavy metal ion in the aqueous solution.

Equation (2) corresponds to a monolayer adsorption with two adsorption sites (i.e., one interaction energy for each adsorption site because its chemical nature is different for each other) [19].

$$q_e = \frac{Ion_{S1} D_{S1}}{1 + \left([Ion]_{hS1} / [Ion]_e \right)^{Ion_{S1}}} + \frac{Ion_{S2} D_{S2}}{1 + \left([Ion]_{hS1} / [Ion]_e \right)^{Ion_{S2}}}, \tag{2}$$

where Ion_{S2}, D_{S2}, and $[Ion]_{hS2}$ are the model parameters for the adsorption site 2. The experimental isotherms of the heavy metal adsorption on hydrochar samples were analyzed with these adsorption models. The interaction energies for the heavy metal ion-adsorption site interface (E_{S1} and E_{S2}, kJ/mol) were calculated with the following equations [19]:

$$E_{S1} = RT \quad \ln\left(\frac{S_{Ion}}{[Ion]_{hS1}} \right),$$

$$E_{S2} = RT \quad \ln\left(\frac{S_{Ion}}{[Ion]_{hS2}} \right), \tag{3}$$

where S_{Ion} is the water solubility (mmol/L) of the salt used to prepare the heavy metal ion solution, R is the universal gas constant, and T is the adsorption temperature (K).

3. Results

3.1. Removal Performance of Tetra Pak-Based Hydrochars and Their Surface Chemistry. Figure 3 shows the results of heavy metal adsorption using the Tetra Pak-based hydrochars

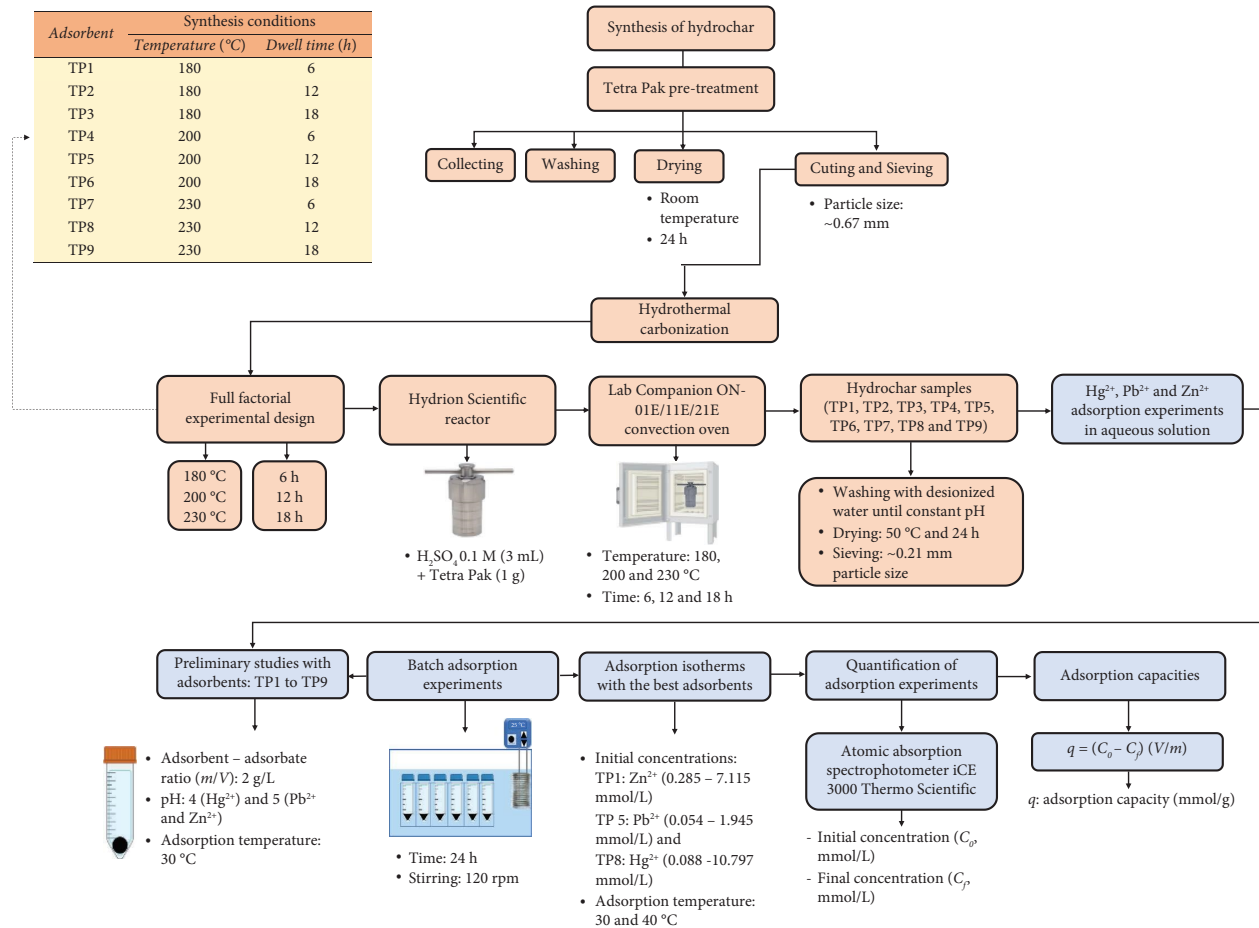| Adsorbent	Synthesis conditions	
	Temperature (°C)	Dwell time (h)
TP1	180	6
TP2	180	12
TP3	180	18
TP4	200	6
TP5	200	12
TP6	200	18
TP7	230	6
TP8	230	12
TP9	230	18

FIGURE 1: Flowchart of the methodology used in the preparation of Tetra Pak-based hydrochars and their evaluation for the depollution of aqueous solutions containing heavy metal ions.
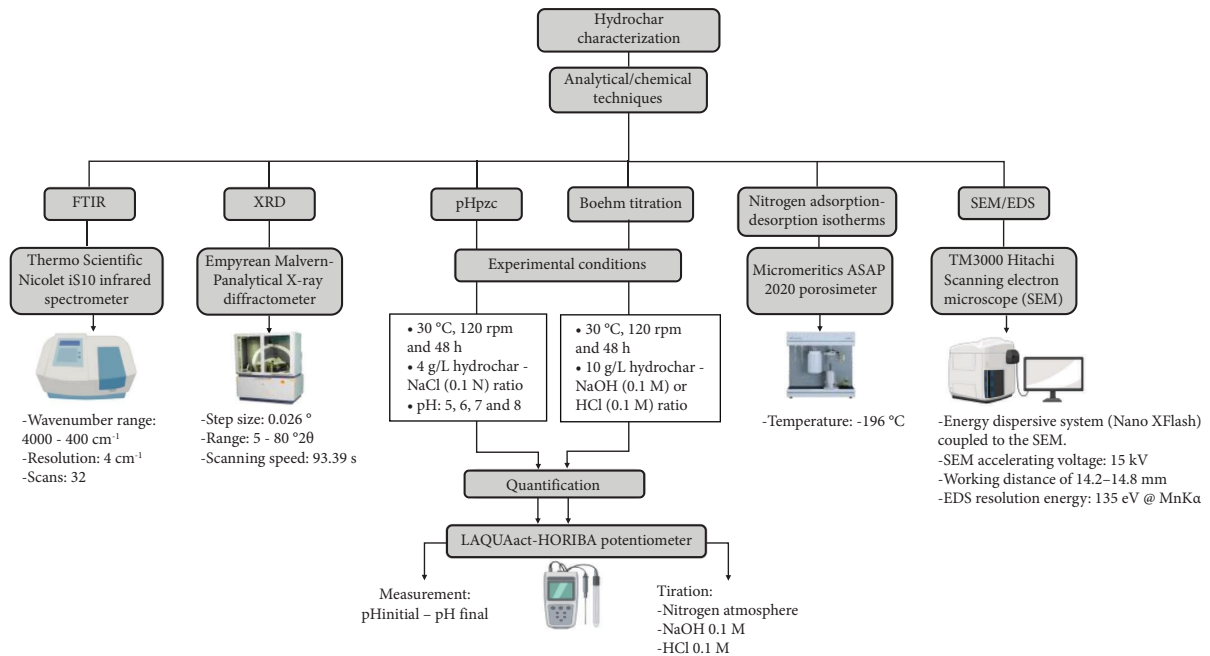

FIGURE 2: Instrumental and analytical techniques applied to characterize the Tetra Pak-based hydrochars.

prepared under different hydrothermal carbonization conditions. The adsorption capacities ranged from 0.015 to 0.063, 0.054 to 0.074, and 0.036 to 0.231 mmol/g for Pb^{2+}, Zn^{2+}, and Hg^{2+}, respectively. The hydrochars showed the best adsorption properties for Hg^{2+} removal, while the lowest removal performance was obtained for Pb^{2+} with all adsorbents. Both the temperature and time of hydrothermal carbonization impacted the adsorption properties of the Tetra Pak hydrochars. It was found that increasing both the hydrothermal carbonization temperature (at 180–230°C) and dwell time (e.g., 6, 12 and 18 h) favored the adsorption properties of these samples to remove Pb^{2+} and Hg^{2+}. These variables significantly affected the Pb^{2+} and Hg^{2+} removal performance of the nine hydrochars, mainly because of their roles in determining the adsorbent composition and surface chemistry. However, these variables had less impact on Zn^{2+} adsorption. Note that the adsorption capacities of Pb^{2+} and Hg^{2+} can vary up to 333 and 533% due to the change in the hydrothermal carbonization conditions, while Zn^{2+} adsorption only changed up to 38%. The best adsorbents for Zn^{2+}, Pb^{2+}, and Hg^{2+} removal were TP1, TP5, and TP8, respectively.

Hydrochar yields ranged from 49 to 94% where the highest and lowest values were obtained for the Tetra Pak hydrothermal carbonization at 180°C for 6 h and 230°C for 18 h, respectively. The increase in hydrothermal carbonization temperature or dwell time caused a gradual degradation of the main components of the Tetra Pak residues, thus affecting the final hydrochar composition. Previous thermogravimetric analyses of Tetra Pak wastes have shown that the cellulose degradation occurs at 280–400°C, while polyethylene degradation starts at >400°C [17]. The yields of the TP1–TP4 samples were 92–94%, while those of the TP5–TP9 samples were 49–55%. These findings agreed with those reported by Muñoz-Batista et al. [17] for the hydrothermal carbonization of Tetra Pak using distilled water. They attributed the differences in the hydrochar yields to the dehydration and degradation of Tetra Pak compounds, mainly cellulose. The degradation of this natural polymer can be accelerated by hydrothermal carbonization in an acidic medium, as reported in this paper. X-ray diffraction patterns of the TP1, TP2, and TP4 hydrochars confirmed the presence of cellulose I, which was identified by the characteristic diffraction peaks at ~15, 22, and 34°2θ [8, 20] (see Figure 4). Although the three samples had the same crystalline structure, their crystallinity and purity were slightly different. On the other hand, TP2, TP5, and TP7 samples displayed the crystalline structure of cellulose I and aluminum silicate hydroxide (ICDD: 00-029-1488). The diffraction pattern of the last component corresponds to the peaks at Bragg angles of ~12.3, 27.9, 35.1, 36.1, 39.2, 44.8, and 55.1°2θ. Aluminum represents approximately 5% of the Tetra Pak composition, and it is exposed once kraft paper decomposition occurs [21]. Crystalline structures of aluminum silicate hydroxide and polyethylene (ICDD: 00-053-1859) were detected in the TP6, TP8, and TP9 samples, suggesting the complete decomposition of cellulose. Lokahita et al. [13] also
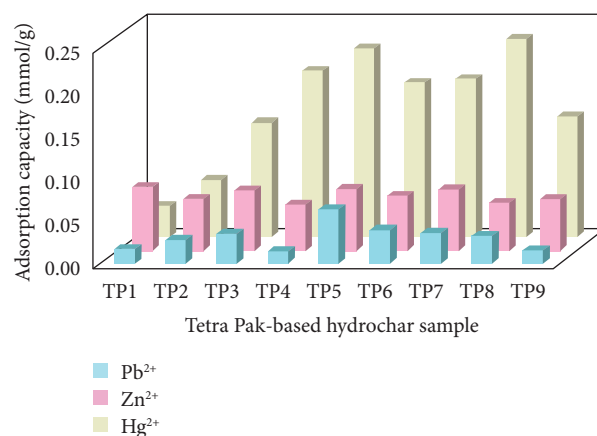

Figure 3: Adsorption capacity of Hg^{2+}, Pb^{2+}, and Zn^{2+} ions from water using hydrochars obtained under different hydrothermal carbonization conditions. The adsorption conditions of the screening tests were 30°C and pH 5 for Pb^{2+} and Zn^{2+} and pH 4 for Hg^{2+}.

concluded that the hydrothermal carbonization with distilled water at >200°C allowed the formation of hydrochar and a composite (aluminum-polyethylene). The shape of the diffraction pattern of the TP5 sample proved that the compositional transition in the hydrochars, caused by the partial degradation of cellulose and polyethylene, occurred at 200°C and dwell time >12 h. Thus, the dwell time of hydrothermal carbonization seems to be more significant than the temperature in the thermal degradation process of the Tetra Pak components.

Tetra Pak-based hydrochars were mainly composed of carbon (C) and oxygen (O) (see Table 2). The C content increased with the hydrothermal carbonization temperature, whereas the O content exhibited the opposite behavior, causing a decrease in the O/C ratio. Therefore, the highest carbonization degree (i.e., dehydration and decarboxylation) was reached for the sample obtained at 230°C for 18 h and with respect to the decrease in temperature as follows: 230 > 200 >> 180°C. C and O elemental compositions of the TP1–TP9 samples agreed with the results reported by Muñoz-Batista et al. [17] for the preparation of hydrochars from Tetra Pak using distilled water. They reported C and O contents of 46–51% and 39–44%, respectively, for hydrochars obtained at 240°C for 40–120 min. In comparison, the chars obtained from Tetra Pak pyrolysis at 400–500°C showed C and O contents of 59–71% and 12–25%, respectively [17]. Lokahita et al. [13] also reported O and C contents of 28–49% and 43–66%, respectively, for Tetra Pak-based hydrochars obtained with distilled water at 200–240°C. The presence of inorganic impurities (i.e., silicon ≤0.4%) in hydrochar samples was confirmed by the EDX analysis (see Table 2). In this case, the presence of silicon is derived from the processing stage of aluminum because some alloying elements (e.g., Cu, Mg, Si, Fe, Mn, and Zn) are usually added to provide specific properties, such as strength and corrosion resistance [22]. Note that the purity of aluminum used in the Tetra Pak containers ranges from 98 to 99 wt% [22].
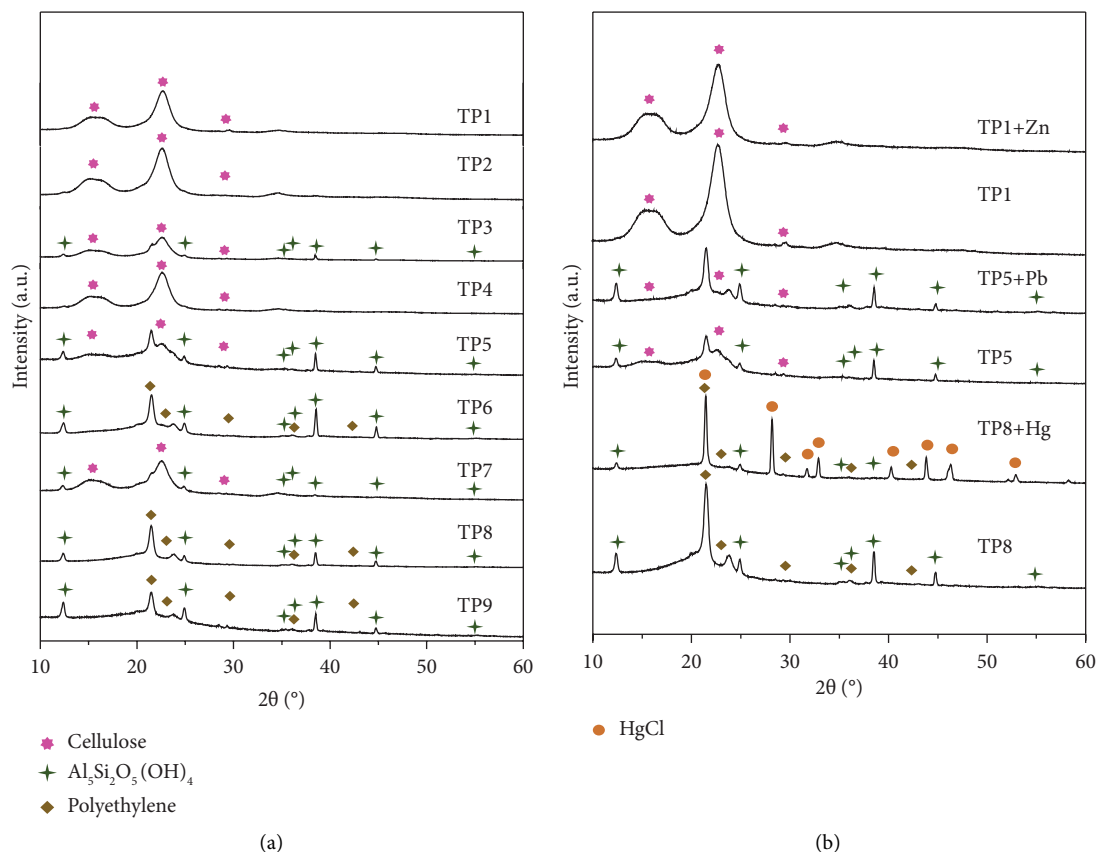
FIGURE 4: Diffraction patterns of Tetra Pak-based hydrochars (a) before and (b) after the adsorption of heavy metal ions from aqueous solutions.

TABLE 2: Surface area and elemental composition of Tetra Pak-based hydrochars.

Hydrochar	Element (wt%)			O/C	S_{BET} (m²/g)
	C	O	Si		
TP1	53	46	—	0.87	<1
TP5	75	24	0.40	0.32	4
TP8	79	21	0.10	0.26	13

The physical changes in the hydrochar samples are shown in Figure 5. SEM micrographs showed that increasing the hydrothermal carbonization temperature and dwell time affected the morphology and physical appearance of these materials. The TP1–TP5 samples had a fibrous appearance, indicating that some noncellulosic moieties were removed by thermochemical conversion [12]. The cellulose fibers in some samples were thin and dispersed along the axial direction. Similar findings have been reported by Xing et al. [12]. TP6–TP9 hydrochar samples exhibited well-defined particles with rough surfaces, suggesting that hydrothermal conversion caused total cellulose degradation to form the hydrochar and aluminum-polyethylene composite. The physical appearance of these hydrochars was also quite different, and their color changed from light brown to dark brown with an increase in the hydrothermal carbonization temperature and dwell time. At a fixed carbonization temperature, the adsorbent became darker as the dwell time increased, indicating a higher degree of degradation of the Tetra Pak compounds. A similar trend was identified with an increase in the carbonization temperature for a fixed dwell time.

Figure 6 provides the infrared spectra of the nine hydrochars. The absorption bands attributed to the O-H (at ~3440 cm^{-1}), C-H (at ~2929–2890 cm^{-1}), C=O (at ~1670–1616, 1450, and 1297 cm^{-1}), and C-O (at ~1037 cm^{-1}) stretching vibrations as well as C-H (at ~1470–1405 cm^{-1}), C-OH (at ~896 cm^{-1}), and C-O (at ~684 cm^{-1}) bending vibrations of diverse functional groups such as β-glycosidic linkages, phenols, alcohols, aliphatic, aromatic, hydroxyl, carbonyl, and/or carboxylic groups were identified in TP1–TP5 samples [8–10, 14, 17, 23]. FTIR spectra of these adsorbents also contained the absorption bands of C-H (at ~1470 cm^{-1}) and C-OH (~1295 cm^{-1}) bonds from CH_2 and phenolic groups from cellulose [8, 9]. The FTIR spectrum of TP5 included an additional small absorption band at ~1703 cm^{-1} attributed to C=O bonds and the deformation of absorption bands at ~1370–1290 cm^{-1}, which resulted in an absorption band at ~1400 cm^{-1} corresponding to the C-H wagging vibration of CH_2 group [10, 17]. FTIR results agreed with the X-ray diffraction analysis, confirming the transition of hydrochar composition from the presence of cellulose to polyethylene, since the characteristic absorption bands of this synthetic polymer were identified [10, 17].
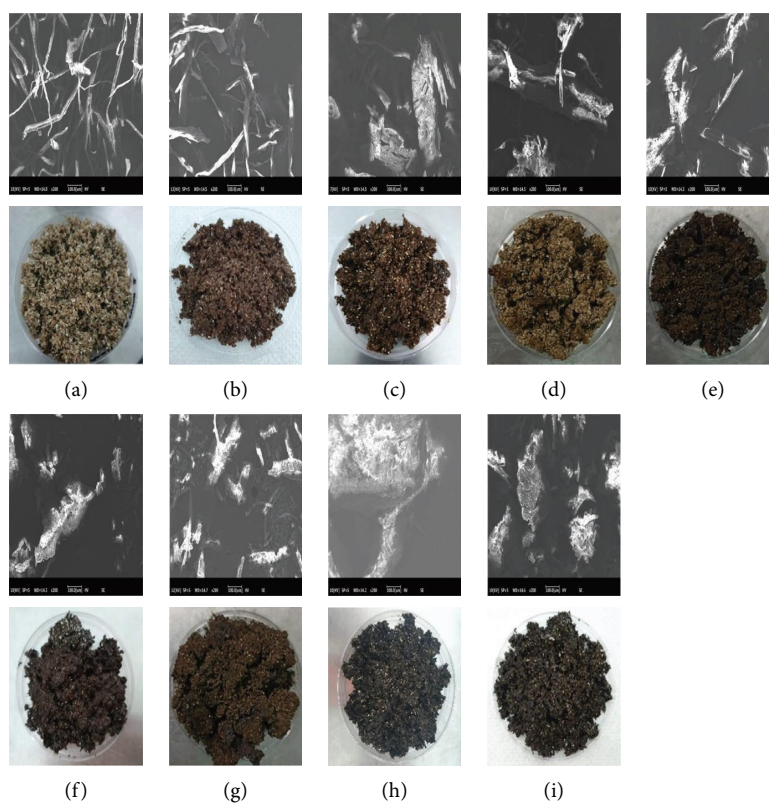
FIGURE 5: SEM images and physical appearance of Tetra Pak-based hydrochar samples obtained under different hydrothermal carbonization conditions. The sample labels are listed in Table 1. (a) TP1; (b) TP2; (c) TP3; (d) TP4; (e) TP5; (f) TP6; (g) TP7; (h) TP8; (i) TP9.

FTIR results of TP5–TP9 indicated the presence of absorption bands at ~3440, 2920–2850, 1703–1614, 1435, 1396, and 1334 cm^{-1} that were related to O-H, C-H, and C=O vibrations or deformations of hydroxyl, methyl, methylene, and carbonyl groups [10, 16, 17, 24]. The absorption bands corresponding to Al-O and/or Si-O bonds were identified at ~1037–960 cm^{-1}, while the absorption bands of Si-O vibrations were located at ~828 and 547 cm^{-1} [25–28]. It was also observed that the intensity and widening of the absorption bands in the FTIR spectra of the samples increased as the temperature and dwell time of hydrothermal carbonization also increased. Muñoz-Batista et al. [17] concluded that these results could also indicate the phase transformation and/or recombination of the Tetra Pak compounds. Therefore, the temperature and dwell time of hydrothermal carbonization determine the degree of degradation of the main components of Tetra Pak wastes [17]. In summary, it was concluded that the Tetra Pak hydrochar samples were composed of a carbon phase, cellulose or polyethylene, and aluminum-silicon moieties (see Table 3). This composition is consistent with the results reported for Tetra Pak chars prepared via pyrolysis [5]. Finally, the concentration of acidic functional groups in the hydrochar samples ranged from 6.2 to 7.9 mmol/g.

All the hydrochar samples were positively charged at pH conditions used in the adsorption studies because of their pH values at point of zero charge (ranging from 6.5 to 7.8) >aqueous solution pH. Consequently, repulsive electrostatic forces occur during the adsorption of these pollutants on hydrochars. Note that the pH values at the point of zero charge of the Tetra Pak-based hydrochars were lower than those of the adsorbent obtained from the slow pyrolysis and acid treatment (i.e., 9.3) of these packing residues [15]. Finally, the surface area of the Tetra Pak hydrochar increased as the hydrothermal carbonization conditions became more severe (Table 2), but all hydrochars can be regarded as low-porosity materials. The surface areas (i.e., 33–174 m^2/g) of Tetra Pak chars prepared via pyrolysis [5, 15] are higher than those of their hydrochar counterparts. The relevance of hydrochar chemistry prevails over the surface area for removing the tested heavy metals.

3.2. Adsorption Isotherms and Removal Mechanism of Tetra Pak-Based Hydrochars. TP1, TP5, and TP8 hydrochar samples were utilized to quantify the adsorption isotherms of Zn^{2+}, Pb^{2+}, and Hg^{2+}, and Figure 7 shows these results. The highest adsorption capacities were obtained for Hg^{2+} (0.24–0.68 mmol/g) using TP8, while the adsorption capacities of TP1 and TP5 to remove Pb^{2+} (0.09–0.11 mmol/g)
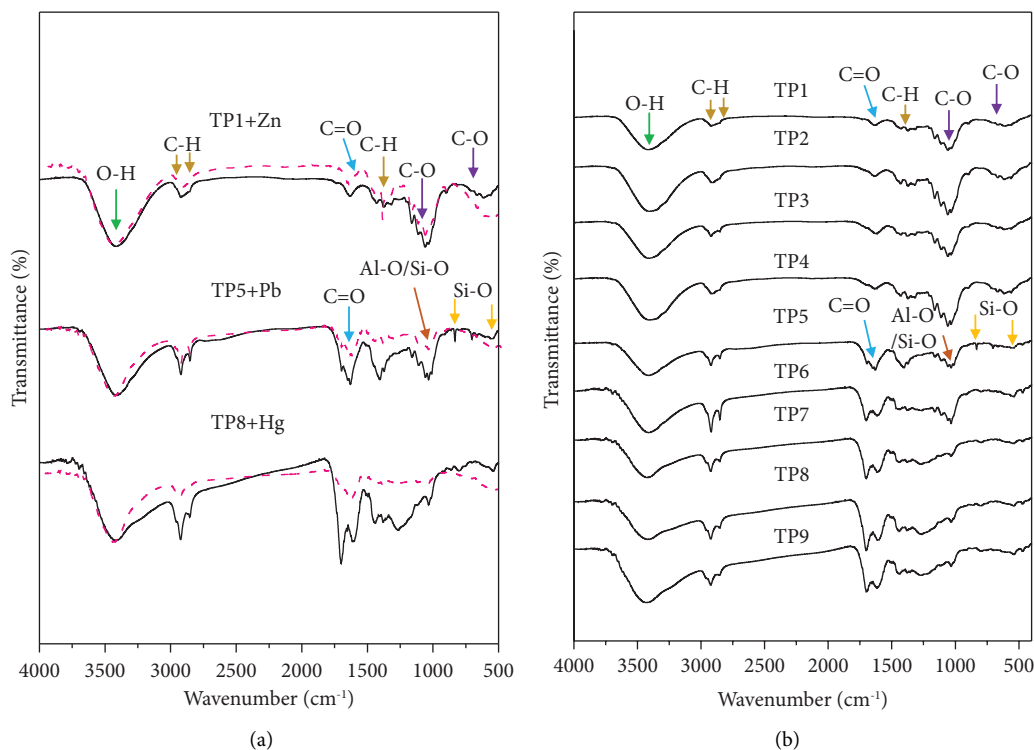
(a)

(b)

FIGURE 6: Infrared spectra of Tetra Pak-based hydrochars (b) before and (a) after the adsorption of heavy metal ions from aqueous solutions.

TABLE 3: Composition of Tetra Pak-based hydrochars prepared under different hydrothermal carbonization conditions.

Hydrochar	Composition
TP1	Carbon phase + cellulose
TP2	Carbon phase + cellulose
TP3	Carbon phase + cellulose + aluminum silicate hydroxide
TP4	Carbon phase + cellulose
TP5	Carbon phase + cellulose + aluminum silicate hydroxide
TP6	Carbon phase + polyethylene + aluminum silicate hydroxide
TP7	Carbon phase + cellulose + aluminum silicate hydroxide
TP8	Carbon phase + polyethylene + aluminum silicate hydroxide
TP9	Carbon phase + aluminum silicate hydroxide

and Zn^{2+} (0.08–0.12 mmol/g) were very similar. All the isotherms displayed the characteristic type 2L shape according to Giles classification for adsorption in liquid phase systems, thus suggesting the affinity of Tetra Pack-based hydrochars towards heavy metal ions [29]. Endothermic adsorption was observed experimentally in the removal of all adsorbates using these hydrochars under the tested experimental conditions. The increment of the aqueous solution temperature from 30 to 40°C improved the adsorption capacities for Zn^{2+}, Pb^{2+}, and Hg^{2+} by 51, 31, and 177%, respectively. The calculated values of enthalpy changes for these adsorption systems were as follows: 34 kJ/mol for TP1-Zn^{2+}, 22 kJ/mol for TP5-Pb^{2+}, and 37 kJ/mol

for TP8-Hg^{2+}, respectively. These ΔH values corresponded to physical interaction forces where electrostatic interactions play a relevant role for the heavy metal adsorption. According to Machado et al. [30], electrostatic forces are involved in the adsorption mechanism for systems with $\Delta H = 20$–80 kJ/mol. A comparison of the adsorption capacities of the hydrochar samples and other biomass-based hydrochars and activated carbons is shown in Figure 8. The adsorption capacities of Tetra Pak hydrochars are competitive and outperformed other adsorbents reported in literature [31–45].

The results of the crystalline structure and surface chemistry analyses of the heavy metal-loaded hydrochars are reported in Figures 4(b) and 6(b), respectively. The intensities of the diffraction peaks associated with TP1 (cellulose) and TP5 (cellulose and aluminum silicate hydroxide) decreased after Zn^{2+} and Pb^{2+} adsorption, but the formation of new crystalline structures was not identified. This behavior also indicated that the removal of these cations was mainly governed by physisorption, which agreed with the thermodynamic calculations. It was also observed that the crystalline structure of TP8 (which was composed of aluminum silicate hydroxide and polyethylene) underwent a drastic change after Hg^{2+} adsorption, and the mercury chloride (ICDD: 00-026-0312) was identified on hydrochar surface. However, some small diffraction peaks ascribed to aluminum silicate (at ~12.3, 24.9, 35.1, and 39.2°2θ) prevailed, indicating the possible participation of aluminum-silicon moieties in the Hg^{2+} removal. Note that the mercury can form amalgams with various metals [46]. For example, Inglezakis et al. [47] reported the removal of mercury using
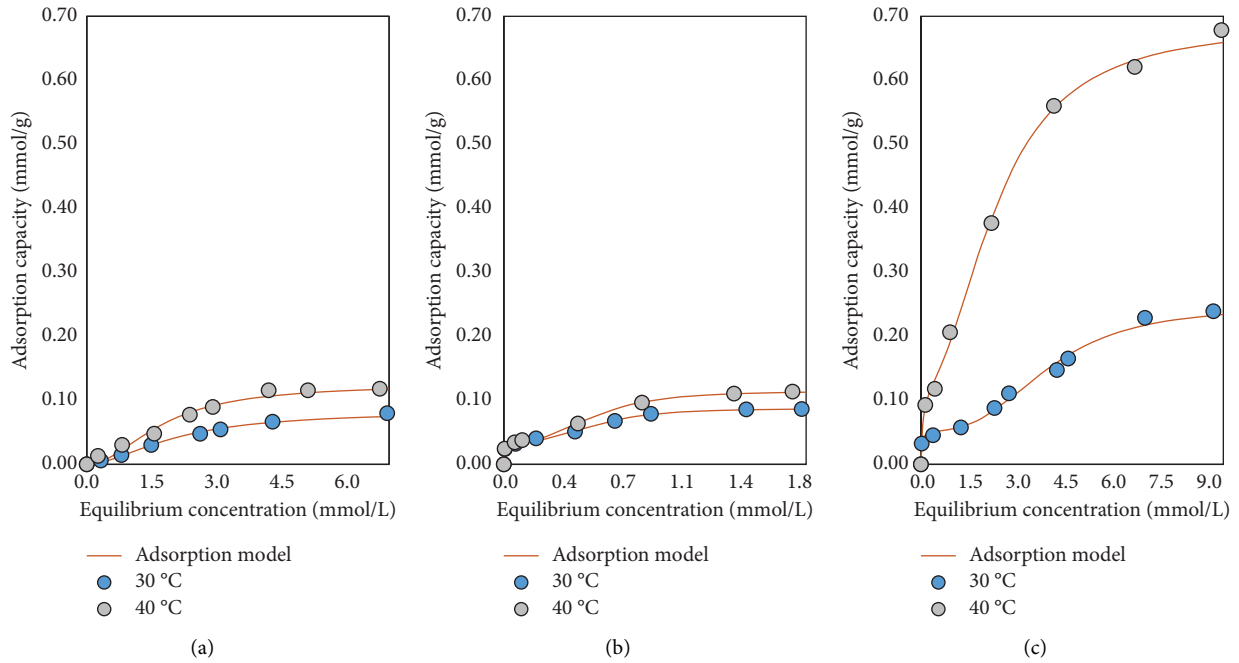
Figure 7: Isotherms of the adsorption of heavy metal ions on the best Tetra Pak-based hydrochars. Experimental conditions: (a, b) pH 5 and (c) pH 4. (a) TP1 hydrochar and Zn^{2+}. (b) TP5 hydrochar and Pb^{2+}. (c) TP8 hydrochar and Hg^{2+}.
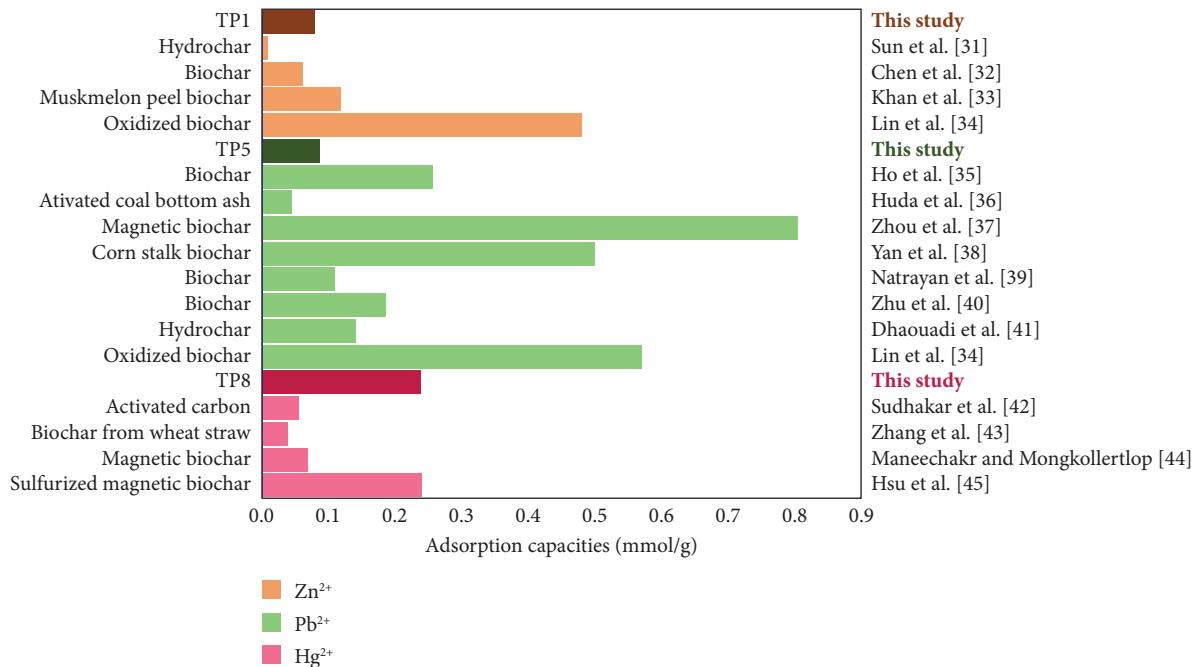

Figure 8: Adsorption capacities of Zn^{2+}, Pb^{2+}, and Hg^{2+} reported in the literature for different adsorbents.

silica containing adsorbents with adsorption capacities up to ~0.5 mmol/g. They suggested the formation of Hg_2Cl_2 on silica materials. Different studies have also demonstrated that the aluminum-containing adsorbents allow the effective removal of mercury ions [48–50].

The infrared spectrum of Zn^{2+}-loaded hydrochar showed that the absorption band at ~3440 cm^{-1} was slightly displaced, the absorption band at ~1450 cm^{-1} disappeared,

and an intense absorption band at ~1390 cm^{-1} was identified. For TP5 loaded with Pb^{2+}, a small displacement in the absorption band at ~3440 cm^{-1} and a decrease in the intensity of the absorption bands located between ~1700 and 1100 cm^{-1} were observed. These changes suggest that Zn^{2+} and Pb^{2+} ions bind to the hydroxyl and carbonyl groups of cellulose and the carbon phase contained in hydrochars [51–54]. Similar results have been reported by Zhan et al.

TABLE 4: Composition of Tetra Pak-based hydrochars prepared under different hydrothermal carbonization conditions.

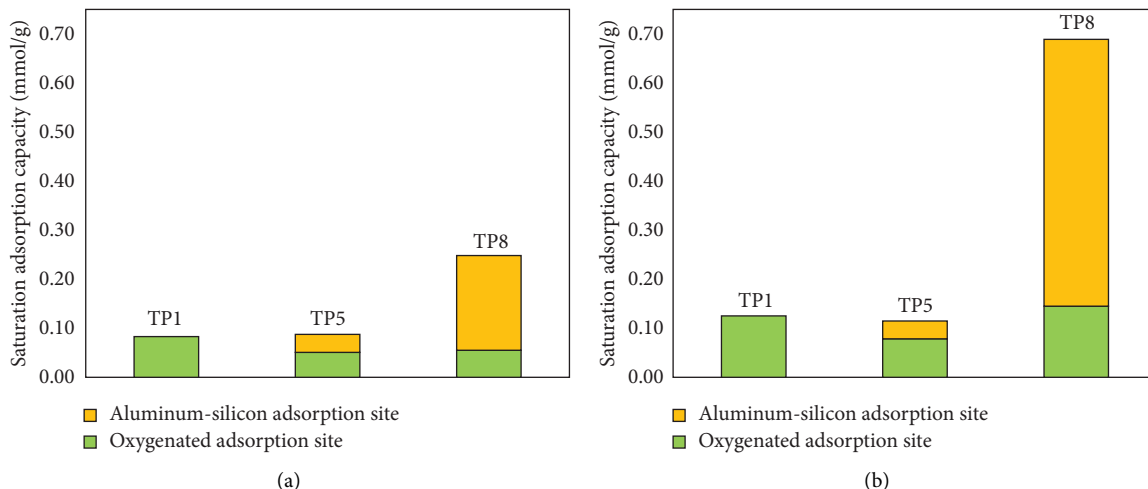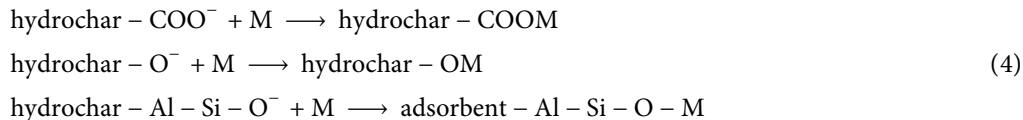| System	T (°C)	Oxygenated site		Aluminum-silicon site	
		Ion_{S1}	D_{S1} (mmol/g)	Ion_{S2}	D_{S2} (mmol/g)
TP1-Zn^{2+}	30	1.8	$4.7E-02$	—	—
	40	2.0	$6.3E-02$	—	—
TP5-Pb^{2+}	30	1.0	$3.8E-02$	3.2	$1.6E-02$
	40	1.3	$2.9E-02$	3.0	$2.6E-02$
TP8-Hg^{2+}	30	0.7	$7.6E-02$	3.0	$6.4E-02$
	40	0.9	$1.6E-01$	2.1	$2.6E-02$

(a)

(b)

FIGURE 9: Contribution of surface functionalities of Tetra Pak-based hydrochars to the adsorption of heavy metal ions from aqueous solutions. (a) 30°C. (b) 40°C.

[55], Xia et al. [56], and Jiang et al. [57] for the Cu^{2+}, Zn^{2+}, and Pb^{2+} adsorption on lignocellulosic adsorbents, hydrochars, and activated carbons. On the other hand, the characterization analysis of hydrochar used in Hg^{2+} adsorption suggested the participation of carbonyl groups and aluminum-silicon moieties in the removal mechanism, as the absorption bands located below $\sim 1700\ cm^{-1}$ underwent a considerable decrease in their intensity [58, 59]. The interactions with oxygenated functionalities and aluminum-silicon moieties for the adsorption of tested metallic ions ($M = Pb^{2+}$, Zn^{2+}, Hg^{2+}) can be described as follows [5, 47, 53, 60, 61]:

$$
\begin{aligned}
&\text{hydrochar} - COO^- + M \longrightarrow \text{hydrochar} - COOM \\
&\text{hydrochar} - O^- + M \longrightarrow \text{hydrochar} - OM \\
&\text{hydrochar} - Al - Si - O^- + M \longrightarrow \text{adsorbent} - Al - Si - O - M
\end{aligned}
\tag{4}
$$

The monolayer model with one adsorption site was used to correlate the Zn^{2+} isotherms of TP1 sample. The characterization results indicated that TP1 has surface functionalities mainly from the carbonaceous phase and cellulose. These functionalities correspond to the oxygenated functional groups that interact with Zn^{2+} ions during adsorption. Consequently, one adsorption site (i.e., oxygenated functional groups for TP1) is involved in the Zn^{2+} removal mechanism. Equation (1) correlated ($R^2 = 0.98$–0.99) the adsorption isotherms of this hydrochar, and the calculated steric parameters are reported in Table 4. On the other hand,

Pb^{2+} and Hg^{2+} adsorption on TP5 and TP8 hydrochars was related to the oxygenated functionalities (from carbonaceous phase and/or cellulose) and the aluminum-silicon moieties. In the case of the TP5 sample, this hydrochar was composed of a carbonaceous phase, cellulose, and aluminum silicate hydroxide, whereas the TP8 hydrochar contained a carbonaceous phase and aluminum silicate hydroxide. Therefore, the adsorption model with two sites, equation (2), fitted ($R^2 > 0.99$) the experimental equilibrium data of the TP5-Pb^{2+} and TP8-Hg^{2+} systems, and the results are also given in Table 4.

Statistical physics modeling indicated that the adsorption of all these heavy metal ions was multi-ionic (i.e., Ion_{S1} and $Ion_{S2} > 1$), where each functional group could interact with a maximum of three cations simultaneously. However, hydrochar surface functionalities play different roles during the removal of these toxic pollutants. The quantity of oxygenated functional groups involved in the removal of these heavy metal ions (D_{S1}) ranged from 0.029 to 0.159 mmol/g, while D_{S2} values for aluminum-silicon moieties were from 0.016 to 0.255 mmol/g. TP8 hydrochar showed the highest concentrations of both adsorption sites. In the case of the TP1 and TP5 samples, the heavy metal ions were bound to the hydrochar surface via oxygenated functional groups (Figure 9). Hg^{2+} was adsorbed mainly (~78%) on the aluminum-silicon adsorption sites of TP8 hydrochar. These calculations confirmed that the temperature and dwell time of the Tetra Pak hydrothermal carbonization significantly affected the composition and surface chemistry of the synthesized hydrochars.

The calculated interaction energies were 21 kJ/mol for Zn^{2+}-oxygenated adsorption site of TP1, 20 and 34 kJ/mol for Pb^{2+}-oxygenated adsorption site and Pb^{2+}-aluminum-silicon moiety of TP5, respectively, and 23 and 11 kJ/mol for Hg^{2+}-oxygenated adsorption site and Hg^{2+}-aluminum-silicon moiety of TP8, respectively. These energy values were consistent with the adsorption mechanisms already described.

4. Conclusions

Hydrothermal carbonization of Tetra Pak wastes generates hydrochars that can be applied as adsorbents to clean water polluted by toxic heavy metals. The hydrothermal carbonization conditions significantly affected the composition and textural parameters of the Tetra Pak-based hydrochars. Low dwell time and carbonization temperature produced hydrochars composed mainly of a carbonaceous phase and cellulose or polyethylene, while hydrochars containing a carbonaceous phase and aluminum silicate hydroxide were obtained at >180°C for >12 h. Hydrochars containing carbonaceous phase + cellulose offer better adsorption properties for Zn^{2+}, while the content of aluminum silicate hydroxide in the hydrochars improves their performance for Pb^{2+} and Hg^{2+} removal. Zinc, lead, and mercury adsorption on Tetra Pak-based hydrochars is a multionic and endothermic process. The preparation of new adsorbents using Tetra Pak residues and hydrothermal carbonization is a promising alternative for sustainable waste management and environmental protection.

Data Availability

The data that support the findings of this study are available from the corresponding author upon reasonable request.

Conflicts of Interest

The authors declare that there are no conflicts of interest.

Acknowledgments

Supplementary Materials

Figure S1. Speciation diagrams of heavy metal ions analyzed in this study. (*Supplementary Materials*)

References

[1] V. Muralidharan, S. Palanivel, and M. Balaraman, "Turning problem into possibility: a comprehensive review on leather solid waste intra-valorization attempts for leather processing," *Journal of Cleaner Production*, vol. 367, Article ID 133021, 2022.

[2] K. A. Oliveira, L. Simão, L. B. Rebouças et al., "Ceramic shell waste valorization: a new approach to increase the sustainability of the precision casting industry from a circular economy perspective," *Waste Management*, vol. 157, pp. 269–278, 2023.

[3] V. Acevedo-García, E. Rosales, A. Puga, M. Pazos, and M. A. Sanromán, "Synthesis and use of efficient adsorbents under the principles of circular economy: waste valorisation and electroadvanced oxidation process regeneration," *Separation and Purification Technology*, vol. 242, Article ID 116796, 2020.

[4] S. Rebello, S. Sali, M. S. Jisha et al., "Chitosan a versatile adsorbent in environmental remediation in the era of circular economy-a mini review," *Sustainable Chemistry and Pharmacy*, vol. 32, Article ID 101004, 2023.

[5] N. M. Zúñiga-Muro, A. Bonilla-Petriciolet, D. I. Mendoza-Castillo et al., "Recycling of Tetra pak wastes via pyrolysis: characterization of solid products and application of the resulting char in the adsorption of mercury from water," *Journal of Cleaner Production*, vol. 291, Article ID 125219, 2021.

[6] S. Matta, M. Bartoli, R. Arrigo, A. Frache, and G. Malucelli, "Flame retardant potential of Tetra Pak®-derived biochar for ethylene-vinyl-acetate copolymers," *Composites Part C: Open Access*, vol. 8, Article ID 100252, 2022.

[7] Y. Wang, Z. Liu, Y. Wang et al., "Catalytic hydrothermal liquefaction of tetra pak with Ni-xCe/CNTs," *Energy*, vol. 261, Article ID 125302, 2022.

[8] C. I. K. Diop and J. M. Lavoie, "Isolation of nanocrystalline cellulose: a technological route for valorizing recycled tetra pak aseptic multilayered food packaging wastes," *Waste and Biomass Valorization*, vol. 8, no. 1, pp. 41–56, 2017.

[9] O. Platnieks, A. Barkane, N. Ijudina, G. Gaidukova, V. K. Thakur, and S. Gaidukovs, "Sustainable tetra pak recycled cellulose/poly(butylene succinate) based woody-like composites for a circular economy," *Journal of Cleaner Production*, vol. 270, Article ID 122321, 2020.

[10] I. Georgiopoulou, G. D. Pappa, S. N. Vouyiouka, and K. Magoulas, "Recycling of post-consumer multilayer Tetra Pak® packaging with the selective dissolution-precipitation process," *Resources, Conservation and Recycling*, vol. 165, Article ID 105268, 2021.

[11] J. Guerra-Garcés, C. A. García-Negrete, K. Pastor-Sierra et al., "Morphologically diverse $CaCO_3$ microparticles and their incorporation into recycled cellulose for circular economy," *Materials Today Sustainability*, vol. 19, Article ID 100166, 2022.

[12] L. Xing, J. Gu, W. Zhang, D. Tu, and C. Hu, "Cellulose I and II nanocrystals produced by sulfuric acid hydrolysis of Tetra pak cellulose I," *Carbohydrate Polymers*, vol. 192, pp. 184–192, 2018.

[13] B. Lokahita, K. Yoshikawa, and F. Takahashi, "Hydrothermal treatment of postconsumer aseptic packaging material: solid fuel production and aluminum recovery," *Energy Procedia*, vol. 105, pp. 610–615, 2017.

[14] X. Chen, Y. Luo, and X. Bai, "Upcycling polyamide containing post-consumer Tetra Pak carton packaging to valuable chemicals and recyclable polymer," *Waste Management*, vol. 131, pp. 423–432, 2021.

[15] Z. Ding, X. Xu, T. Phan, X. Hu, and G. Nie, "High adsorption performance for as (III) and as (V) onto novel aluminum-enriched biochar derived from abandoned Tetra Paks," *Chemosphere*, vol. 208, pp. 800–807, 2018.

[16] G. G. Şahin and M. Karaboyacı, "Process and machinery design for the recycling of tetra pak components," *Journal of Cleaner Production*, vol. 323, Article ID 129186, 2021.

[17] M. J. Muñoz-Batista, G. Blázquez, J. F. Franco, M. Calero, and M. A. Martín-Lara, "Recovery, separation and production of fuel, plastic and aluminum from the Tetra PAK waste to hydrothermal and pyrolysis processes," *Waste Management*, vol. 137, pp. 179–189, 2022.

[18] D. Zmijková, B. Švédová, and J. Růžičková, "Polycyclic aromatic hydrocarbons in biochar originated from pyrolysis of aseptic packages (Tetra Pak®)," *Sustainable Chemistry and Pharmacy*, vol. 27, Article ID 100682, 2022.

[19] O. Amrhar, L. El Gana, and M. Mobarak, "Calculation of adsorption isotherms by statistical physics models: a review," *Environmental Chemistry Letters*, vol. 19, no. 6, pp. 4519–4547, 2021.

[20] D. Akgün, D. Ova Özcan, and B. Övez, "Optimization and characterization of cellulose nanocrystal production from aseptic tetra pak food packaging waste," *Journal of the Turkish Chemical Society Section A: Chemistry*, vol. 9, no. 1, pp. 131–148, 2022.

[21] A. Korkmaz, J. Yanik, M. Brebu, and C. Vasile, "Pyrolysis of the tetra pak," *Waste Management*, vol. 29, no. 11, pp. 2836–2841, 2009.

[22] G. Martínez-Barrera, A. L. de la Colina-Martínez, M. Martínez-López et al., "Recovery and reuse of waste tetra pak packages by using a novel treatment," *Trends in Beverage Packaging*, vol. 16, pp. 303–341, 2019.

[23] S. Yuan, J. J. Zhang, H. X. Fan, and X. H. Dai, "Facile and sustainable shear mixing/carbonization approach for upcycling of carton into superhydrophobic coating for efficient oil-water separation," *Journal of Cleaner Production*, vol. 196, pp. 644–652, 2018.

[24] M. R. Jung, F. D. Horgen, S. V. Orski et al., "Validation of ATR FT-IR to identify polymers of plastic marine debris, including those ingested by marine organisms," *Marine Pollution Bulletin*, vol. 127, pp. 704–716, 2018.

[25] N. Ariffin, M. M. A. B. Abdullah, P. Postawa et al., "Effect of aluminium powder on kaolin-based geopolymer characteristic and removal of Cu^{2+}," *Materials*, vol. 14, no. 4, p. 814, 2021.

[26] A. Herrera-Barros, C. Tejada-Tovar, and A. D. Gonzalez-Delgado, "Comparative assessment of Al_2O_3 modified biomasses from agricultural residues for nickel and cadmium removal," *Journal of Water and Land Development*, vol. 49, pp. 29–34, 2021.

[27] D. Sachan, A. Ramesh, and G. Das, "Green synthesis of silica nanoparticles from leaf biomass and its application to remove heavy metals from synthetic wastewater: a comparative analysis," *Environmental Nanotechnology, Monitoring & Management*, vol. 16, Article ID 100467, 2021.

[28] J. Nyirenda, G. Kalaba, and O. Munyati, "Synthesis and characterization of an activated carbon-supported silver-silica nanocomposite for adsorption of heavy metal ions from water," *Results in Engineering*, vol. 15, Article ID 100553, 2022.

[29] C. H. Giles, T. H. MacEwan, S. N. Nakhwa, and D. Smith, "786. Studies in adsorption. Part XI. A system of classification of solution adsorption isotherms, and its use in diagnosis of adsorption mechanisms and in measurement of specific surface areas of solids," *Journal of the Chemical Society*, vol. 14, pp. 3973–3993, 1960.

[30] F. M. Machado, C. P. Bergmann, E. C. Lima et al., "Adsorption of reactive blue 4 dye from water solutions by carbon nanotubes: experiment and theory," *Physical Chemistry Chemical Physics*, vol. 14, no. 31, pp. 11139–11153, 2012.

[31] K. Sun, J. Tang, Y. Gong, and H. Zhang, "Characterization of potassium hydroxide (KOH) modified hydrochars from different feedstocks for enhanced removal of heavy metals from water," *Environmental Science & Pollution Research*, vol. 22, no. 21, pp. 16640–16651, 2015.

[32] X. Chen, G. Chen, L. Chen et al., "Adsorption of copper and zinc by biochars produced from pyrolysis of hardwood and corn straw in aqueous solution," *Bioresource Technology*, vol. 102, no. 19, pp. 8877–8884, 2011.

[33] T. A. Khan, A. A. Mukhlif, and E. A. Khan, "Uptake of Cu^{2+} and Zn^{2+} from simulated wastewater using muskmelon peel biochar: isotherm and kinetic studies," *Egyptian Journal of Basic and Applied Sciences*, vol. 4, no. 3, pp. 236–248, 2017.

[34] S. Lin, W. Huang, H. Yang, S. Sun, and J. Yu, "Recycling application of waste long-root *Eichhornia crassipes* in the heavy metal removal using oxidized biochar derived as adsorbents," *Bioresource Technology*, vol. 314, Article ID 123749, 2020.

[35] S. H. Ho, Y. D. Chen, Z. K. Yang, D. Nagarajan, J. S. Chang, and N. Ren, "High-efficiency removal of lead from wastewater by biochar derived from anaerobic digestion sludge," *Bioresource Technology*, vol. 246, pp. 142–149, 2017.

[36] B. N. Huda, E. T. Wahyuni, Y. Kamiya, and M. Mudasir, "Kinetic and thermodynamic study on adsorption of lead (II) ions in water over dithizone-immobilized coal bottom ash," *Materials Chemistry and Physics*, vol. 282, Article ID 126005, 2022.

[37] X. Zhou, Y. Liu, J. Zhou, J. Guo, J. Ren, and F. Zhou, "Efficient removal of lead from aqueous solution by urea-functionalized magnetic biochar: preparation, characterization and mechanism study," *Journal of the Taiwan Institute of Chemical Engineers*, vol. 91, pp. 457–467, 2018.

[38] S. Yan, W. Yu, T. Yang, Q. Li, and J. Guo, "The adsorption of corn stalk biochar for Pb and Cd: preparation, characterization, and batch adsorption study," *Separations*, vol. 9, no. 2, p. 22, 2022.

[39] L. Natrayan, S. Kaliappan, C. N. Dheeraj Kumar Reddy et al., "Development and characterization of carbon-based adsorbents derived from agricultural wastes and their effectiveness in adsorption of heavy metals in waste water," *Bioinorganic Chemistry and Applications*, vol. 2022, Article ID 1659855, 18 pages, 2022.

[40] S. Zhu, S. Ho, X. Huang et al., "Magnetic nanoscale zerovalent iron assisted biochar: interfacial chemical behaviors and heavy metals remediation performance," *ACS Sustainable Chemistry & Engineering*, vol. 5, no. 11, pp. 9673–9682, 2017.

[41] F. Dhaouadi, L. Sellaoui, L. E. Hernández-Hernández et al., "Preparation of an avocado seed hydrochar and its application as heavy metal adsorbent: properties and advanced statistical physics modeling," *Chemical Engineering Journal*, vol. 419, Article ID 129472, 2021.

[42] M. Sudhakar, V. S. Reddy, S. Mekala, and K. Ravindhranath, "Effective bio-sorbents for the simultaneous removal of cadmium and mercury ions from polluted waters: based on ficus panda plant areal roots active carbon, nano particle of SnO_2 and Al-alginate beads," *Journal of Polymers and the Environment*, vol. 31, no. 5, pp. 2032–2054, 2022.

[43] S. Zhang, X. Yang, M. Ju, L. Liu, and K. Zheng, "Mercury adsorption to aged biochar and its management in China," *Environmental Science & Pollution Research*, vol. 26, no. 5, pp. 4867–4877, 2019.

[44] P. Maneechakr and S. Mongkollertlop, "Investigation on adsorption behaviors of heavy metal ions (Cd^{2+}, Cr^{3+}, Hg^{2+} and Pb^{2+}) through low-cost/active manganese dioxide-modified magnetic biochar derived from palm Zhang kernel cake residue," *Journal of Environmental Chemical Engineering*, vol. 8, no. 6, Article ID 104467, 2020.

[45] C. J. Hsu, Y. H. Cheng, Y. P. Huang, J. D. Atkinson, and H. C. Hsi, "A novel synthesis of sulfurized magnetic biochar for aqueous Hg (II) capture as a potential method for environmental remediation in water," *The Science of the Total Environment*, vol. 784, Article ID 147240, 2021.

[46] J. R. Magkert, "Dental amalgam and mercury," *Journal of The American Dental Association*, vol. 122, no. 8, pp. 54–61, 1991.

[47] V. J. Inglezakis, S. Azat, Z. Tauanov, and S. V. Mikhalovsky, "Functionalization of biosourced silica and surface reactions with mercury in aqueous solutions," *Chemical Engineering Journal*, vol. 423, Article ID 129745, 2021.

[48] S. M. Bachand, T. E. C. Kraus, D. Stern, Y. L. Liang, W. R. Horwath, and P. A. M. Bachand, "Aluminum- and iron-based coagulation for in-situ removal of dissolved organic carbon, disinfection byproducts, mercury and other constituents from agricultural drain water," *Ecological Engineering*, vol. 134, pp. 26–38, 2019.

[49] K. Deliz Quiñones, A. Hovsepyan, A. Oppong-Anane, and J. C. J. Bonzongo, "Insights into the mechanisms of mercury sorption onto aluminum based drinking water treatment residuals," *Journal of Hazardous Materials*, vol. 307, pp. 184–192, 2016.

[50] K. G. Pavithra, P. SundarRajan, P. S. Kumar, and G. Rangasamy, "Mercury sources, contaminations, mercury cycle, detection and treatment techniques: a review," *Chemosphere*, vol. 312, Article ID 137314, 2023.

[51] M. Li, S. A. Messele, Y. Boluk, and M. Gamal El-Din, "Isolated cellulose nanofibers for Cu (II) and Zn (II) removal: performance and mechanisms," *Carbohydrate Polymers*, vol. 221, pp. 231–241, 2019.

[52] M. Zhao, Y. Dai, M. Zhang et al., "Mechanisms of Pb and/or Zn adsorption by different biochars: biochar characteristics, stability, and binding energies," *The Science of the Total Environment*, vol. 717, Article ID 136894, 2020.

[53] V. P. Dinh, D. K. Nguyen, T. T. Luu et al., "Adsorption of Pb (II) from aqueous solution by pomelo fruit peel-derived biochar," *Materials Chemistry and Physics*, vol. 285, Article ID 126105, 2022.

[54] S. Zhao, H. Luo, A. Ma, W. Xie, K. Sun, and Z. Sun, "Influence of pyrolysis conditions on the mercury removal characteristics and physicochemical properties of biomass coke," *Fuel*, vol. 313, Article ID 122979, 2022.

[55] W. Zhan, C. Xu, G. Qian, G. Huang, X. Tang, and B. Lin, "Adsorption of Cu(II), Zn(II), and Pb(II) from aqueous single and binary metal solutions by regenerated cellulose and sodium alginate chemically modified with polyethyleneimine," *RSC Advances*, vol. 8, no. 33, pp. 18723–18733, 2018.

[56] Y. Xia, T. Yang, N. Zhu et al., "Enhanced adsorption of Pb (II) onto modified hydrochar: modeling and mechanism analysis," *Bioresource Technology*, vol. 288, Article ID 121593, 2019.

[57] L. Jiang, Y. Chen, Y. Wang et al., "Contributions of various Cd(II) adsorption mechanisms by *Phragmites australis*-activated carbon modified with mannitol," *ACS Omega*, vol. 7, no. 12, pp. 10502–10515, 2022.

[58] Q. Zhou, Y. Duan, C. Zhu et al., "Adsorption equilibrium, kinetics and mechanism studies of mercury on coal-fired fly ash," *Korean Journal of Chemical Engineering*, vol. 32, no. 7, pp. 1405–1413, 2015.

[59] E. Elkhatib, M. Moharem, A. Mahdy, and M. Mesalem, "Sorption, release and forms of mercury in contaminated soils stabilized with water treatment residual nanoparticles," *Land Degradation & Development*, vol. 28, no. 2, pp. 752–761, 2016.

[60] M. C. Gabriel and D. G. Williamson, "Principal biogeochemical factors affecting the speciation and transport of mercury through the terrestrial environment," *Environmental Geochemistry and Health*, vol. 26, no. 3-4, pp. 421–434, 2004.

[61] A. K. Sakhiya, P. Baghel, A. Anand, V. K. Vijay, and P. Kaushal, "A comparative study of physical and chemical activation of rice straw derived biochar to enhance Zn^{2+} adsorption," *Bioresource Technology Reports*, vol. 15, Article ID 100774, 2021.